Bubble Coalescence and Break-Up in Air-Sparged Bubble Columns

A phenomenological model is proposed for the rates of bubble coalescence and bubble break-up in turbulent gas-liquid dispersions. Bubble coalescence is modeled by considering bubble collisions due to turbulence, buoyancy, and laminar shear, and by analysis of the coalescence efficiency of collisions. Bubble break-up is analyzed in terms of bubble interactions with turbulent eddies. A method for the measurement of coalescence and break-up events in turbulent systems is described and used to test the validity of the proposed model. The measurement technique relies on the mixing of tracer gases within bubbles upon coalescence, in conjunction with Monte-Carlo simulations of coalescence events. Both distilled water and salt solutions are examined. Favorable agreement is found between the model and the individual coalescence and breakage rates, as well as with data obtained for the average bubble size and bubble size distribution.

Michael J. Prince
Harvey W. Blanch
Department of Chemical Engineering
University of California
Berkeley, CA 94720

Introduction

Gas-liquid contactors find broad application as reactors and separation units in the chemical, mining, pharmaceutical and biochemical industries. In these systems the rate of transport of the gas to the liquid phase often limits productivity and is therefore a critical design criterion. Current design methods rely on empirical correlations which may not be confidently applied beyond the narrow range of operating conditions and geometries over which they were determined.

The uncertainty in bubble column design arises from a lack of fundamental understanding of the hydrodynamics and rate processes which govern bubble size and thus interfacial area. Bubble size depends on a balance of coalescence and break-up rates in the vessel. No broadly applicable model for these rate processes in turbulent systems has yet been presented. This has been due to the inability to measure bubble coalescence and break-up in systems where high gas flow rates prevent direct visual observation.

The objective of this study is to measure bubble coalescence and break-up rates in turbulent gas-liquid dispersions and to develop a model for these rate processes based on physicochemical and hydrodynamic principles. The ability of the model to adequately predict the individual experimental rate of coalescence and break-up is used to judge its validity. In addition, the model is tested against its ability to predict bubble size and bubble size distributions.

The coalescence process is analyzed by examination of bubble collision events and the likelihood of collisions resulting in coalescence. Bubble break-up is examined in terms of bubble interactions with turbulent eddies. In addition to the theoretical development, an experimental method for the measurement of bubble coalescence and break-up rates in turbulent systems is described.

The effect of inorganic electrolytes on coalescence and break-up rates is also examined. Much of the current interest in the prediction of bubble size stems from the desire to predict oxygen transfer rates in aerobic biochemical reactors. In these systems the liquid media typically contains inorganic electrolytes which provide minerals for microbial growth. Other applications where salts influence bubble size are mineral flotation and treatment of polluted saline waters.

The addition of inorganic electrolytes has been found to have a marked effect on bubble size by a number of investigators (Marrucci and Nicodemo, 1967; Keitel and Onken, 1982; Oolman and Blanch, 1986a). Changes in bubble size may result from the influence of salts on either bubble break-up or bubble coalescence rates. In this work the degree to which each of these mechanisms is affected by salt concentration is examined and a model is developed to predict these rate processes in inorganic electrolyte solutions. While inorganic salts are only one form of

Current address of M. J. Prince: Department of Chemical Engineering, Bucknell University, Lewisburg, PA 17837.

surface contaminant, the analysis for other compounds which affect the surface tension will be similar in many respects.

Model Development

Bubble coalescence

Previous experimental studies on bubble coalescence fall into one of two categories; measurement of coalescence times in stagnant liquids (Marrucci, 1969; Kim and Lee, 1987), or determination of coalescence rates from bubble size data obtained in turbulent systems (Calderbank et al., 1964). Neither approach is satisfactory for determining the rate of coalescence under practical hydrodynamic conditions. Film thinning times in stagnant liquids cannot be used to determine coalescence rates in more complex hydrodynamic environments. Similarly, measurement of bubble sizes in turbulent flows does not provide information on the independent contributions of break-up and coalescence rates, both of which determine bubble size. While various models consider these rate processes independently for the case of liquid-liquid systems (Coulaloglou and Tavlarides, 1977; Ross et al., 1978; Valentas and Amundson, 1966), these models have not been tested due to a lack of experimental data on the individual rate processes. There are also differences in behavior between liquid-liquid and gas-liquid systems which must be considered in modeling bubble coalescence and break-up.

Coalescence of two bubbles in turbulent flows occurs in three steps. First, bubbles collide, trapping a small amount of liquid between them. This liquid then drains until the liquid film separating the bubbles reaches a critical thickness. At this point, film rupture occurs resulting in coalescence. From the first step, it is seen that the coalescence rate is intimately connected to the collision rate. In order to determine whether a given collision will result in coalescence, it is necessary to determine the collision efficiency. Two bubbles will coalesce provided they remain in contact for a period of time sufficient for the liquid film between them to thin to the critical value necessary for rupture.

Collisions may occur due to a variety of mechanisms. We shall consider collisions arising from turbulence, buoyancy and laminar shear. It is clear that collisions may result from the random motion of bubbles due to turbulence. In addition, bubbles of different sizes will have different rise velocities which may lead to collision. Finally, bubbles located in a region of relatively high liquid velocity may collide with bubbles in a slower section of the velocity field. It is assumed that collisions from these various mechanisms are cumulative. In support of this, Swift and Friedlander (1964) have reported the cumulative collisions of aerosol particles from Brownian motion and laminar shear. The collision mechanisms described will be examined in turn.

Turbulent collision rate

A primary cause of bubble collisions is the fluctuating turbulent velocity of the liquid phase. Collision takes place by a mechanism analogous to particle collisions in an ideal gas. Following Kennard (1938), the collision frequency resulting from turbulent motion (θ_{ij}^T) can be expressed as a function of bubble size, concentration and velocity:

$$\theta_{ij}^T = n_i n_j S_{ij} (\bar{u}_{ti}^2 + \bar{u}_{tj}^2)^{1/2} \tag{1}$$

where n_i and n_j are the concentrations of bubbles of radius r_{bi} and r_{bj}, respectively, $\bar{u}_t$ is the average turbulent fluctuating velocity of the bubble and S_{ij} is the collision cross-sectional area of the bubbles defined by:

$$S_{ij} = \frac{\pi}{4} (r_{bi} + r_{bj})^2 \tag{2}$$

The velocity of bubbles in Eq. 1 is assumed to be the turbulent eddy velocity of the length scale of the bubble. Eddy motion of this scale is primarily responsible for the relative motion between bubbles. Very small eddies do not contain sufficient energy to significantly affect bubble motion, while eddies much larger than the bubble size transport groups of bubbles without leading to significant relative motion. Determination of a value for the turbulent velocity of a bubble requires somewhat restrictive assumptions about the nature of the turbulent field. It is customary to assume that the turbulence is isotropic and that the bubble size lies in the inertial subrange. Both of these assumptions are necessary in order to make the problem tractable. Even if the turbulence is not strictly isotropic, the assumption of isotropic turbulence may still prove useful if isotropy exists at the length scale of the bubble diameter. This is a less restrictive assumption than isotropy throughout the entire length spectrum. In addition, isotropic modeling may be considered an approximate solution to systems that are mildly nonisotropic.

The second assumption in determining the turbulent velocity of the bubble is that the bubble size lies in the inertial subrange. This criteria is typically examined in terms of the inverse radius or wave number. The criteria for the inertial subrange is that:

$$k_e \ll k_b \ll k_d \tag{3}$$

where k_e is the wave number of the large energy containing eddies, k_b is the wave number corresponding to the bubble size and k_d is the wave number of the eddies of viscous dissipation. The wave number for energy dissipation, equivalent to the inverse of the microscale of turbulence, is defined by Batchelor (1953) as:

$$k_d = 0.5 \frac{\epsilon^{1/4}}{\nu^{3/4}} \tag{4}$$

where ϵ is the energy dissipation per unit mass and ν is the kinematic viscosity. Bhavaraju et al. (1978) developed an expression for the power input (Ψ) to gas sparged vessels based on the expansion of bubbles as they ascend the column from pressure P_2 to P_1, at volumetric gas flow rate Q:

$$\Psi = QP_2 \frac{\ln (P_1/P_2)}{P_1 - P_2} \rho_l g H_T \tag{5}$$

This expression is divided by the mass of the system to give ϵ.

$$\epsilon = \frac{Qg}{\pi R_T^2} \frac{P_2 \ln (P_1/P_2)}{(P_1 - P_2)}; \quad P_1 = P_2 + \rho_l g H_T \tag{6}$$

In these expressions H_T is the unaerated height of liquid and R_T

is the radius of the column. The kinetic energy and mass of the gas phase have been neglected in this formulation.

It is now possible to examine the conditions outlined in Eq. 3. Using Eqs. 4 and 6, the microscale of turbulence is approximately 0.01 centimeters over the experimental range of gas flow rates employed in the present study. The size of the energy containing eddies is typically assumed to be equal to the vessel diameter. The bubble column employed in the present study had a diameter of 27 cm. Typical bubble sizes in turbulent gas-sparged contactors are approximately 0.4 cm. Thus the length scale of the bubble is well removed from that of both the energy containing eddies and eddies of viscous dissipation and falls in the inertial subrange as defined by Eq. 3. This situation will similarly apply in most industrial scale contactors.

The turbulent velocity in the inertial subrange of isotropic turbulence is (Rotta, 1972):

$$u_t = 1.4\epsilon^{(1/3)} d_b^{(1/3)} \tag{7}$$

where d_b is the bubble diameter. Substitution of this value into Eq. 1 yields the turbulent collision rate.

$$\theta_{ij}^{T} = 0.089\pi n_i n_j (d_{bi} + d_{bj})^2 \epsilon^{1/3} (d_{bi}^{2/3} + d_{bj}^{2/3})^{1/2} \tag{8}$$

A similar expression for liquid-liquid systems is found in Coulaloglou and Tavlarides (1977) with a small algebraic error.

Buoyancy-driven collision rates

Collisions may result from the difference in rise velocities of bubbles of different size. The buoyant collision rate (θ_{ij}^{B}) is given by Friedlander (1977):

$$\theta_{ij}^{B} = n_i n_j S_{ij} (u_{r_i} - u_{r_j}) \tag{9}$$

Here u_r is the rise velocity of the particle. The rise velocity can be expressed as a function of size. Clift et al. (1978) provide an expression that covers the size range typical of gas-liquid contactors operating in the turbulent flow regime:

$$u_r = [(2.14\sigma)/\rho_l d_b + 0.505 g d_b]^{1/2} \tag{10}$$

Where ρ_l is the liquid density and σ is the surface tension. The equation is strictly applicable only to uncontaminated bubbles with mobile gas-liquid interfaces. It is employed in the present work since the liquid phase is distilled water. The use of distilled water does not guarantee a completely mobile interface, however, the error in the collision frequency from using this equation will be slight.

Laminar shear collision rate

The final contribution to the collision rate results from laminar shear in the liquid phase. Collisions occur in this situation as a result of the development of a gross circulation pattern in a bubble column at sufficiently high gas rates. It is well recognized that a bubble column may operate under a variety of hydrodynamic regimes (Shah and Deckwer, 1983). At low gas flow rates, gas is evenly distributed radially throughout the vessel. At higher gas flow rates, bubbles begin to preferentially rise through the center of the column. The result is the development of a gross circulation pattern with a net upward velocity in the column center and down flow in the outer annular region near the wall.

This circulation pattern also gives rise to a radial velocity distribution. Because of this, it is possible for bubbles situated in a zone of relatively high liquid velocity to overtake another bubble of the same size and rise velocity. The functional form of the collision rate due to laminar shear (θ_{ij}^{LS}) is given by Friedlander (1977) as:

$$\theta_{ij}^{LS} = n_i n_j \frac{4}{3} (r_{b_i} + r_{b_j})^3 \left(\frac{\overline{dU_l}}{dR}\right) \tag{11}$$

where U_l is the liquid circulation velocity and R is the radial coordinate of the column. The final term in Eq. 11 is the average shear rate.

To evaluate the average shear rate, we shall use the velocity profile developed by Walters and Blanch (1983) for inviscid systems. The exact velocity profile is a function of the position of the stagnation point, the radial distance at which there is no net upward or downward flow. For inviscid systems, Walters and Blanch state that the transition point occurs at a radial position of approximately $0.7R_T$. The velocity profile for this condition is:

$$U_l = U_{l,\max} [1 - R^2/(\alpha R_T)^2] \tag{12}$$

Here αR_T is the transition point and $U_{l,\max}$ is the velocity in the center of the column. Note that Eq. 12 is not strictly accurate at the walls of the column, where a no slip condition requires a value of zero for the velocity. However, as described in Walters and Blanch, Eq. 12 provides a good estimate for inviscid systems where the boundary layer at the column wall is quite thin. The mean shear rate is found by averaging the local shear rate over the radial dimension of the column. If we substitute $\gamma(R)$ for the local shear rate we find:

$$\overline{\gamma}(R) = \frac{|2\int_0^{\alpha R_T} \gamma(R) \cdot R dR|}{(\alpha R_T)^2} + \frac{|2\int_{\alpha R_T}^{R_T} \gamma(R) \cdot R dR|}{R_T^2(1 - \alpha^2)} = 5.3 \frac{U_{l,\max}}{R_T} \tag{13}$$

Collisions due to laminar shear occur if the bubble column operates in the heterogeneous regime where the nonuniform gas holdup produces a circulation profile. The transition from the homogeneous regime is taken to occur at a superficial gas velocity of 4.0 cm/s (Ueyama and Miyauchi, 1979). In addition, Shah and Deckwer report a large transition zone before fully developed heterogeneous flow appears. In the present study, the superficial gas rates employed range from 0.58 to 5.2 cm/s. Consequently, this mechanism of collision will not play a significant role at the relatively low gas rates employed. However, many industrial bubble columns operate in the heterogeneous regime where this collision mechanism may need to be considered.

The model of Miyauchi and Shyu (1970) was used to predict the maximum circulating velocity for the gas sparge rates above 4.0 cm/s. The center line liquid circulation velocity in this case

is thus given by:

$$U_{l,\max} = \left(\frac{1 - 0.75\phi}{1 - \phi}\right)\frac{\phi g D_T^2}{48\nu_t} \tag{14}$$

Here ϕ is the gas hold-up and ν_t is the turbulent kinetic viscosity given by:

$$\nu_t = 0.0536\,\frac{D_T^{1.77}}{\rho_l} \tag{15}$$

Substitution of Eqs. 13 and 14 into Eq. 11 yields a value for the laminar shear collision rate.

Collision efficiency

In order to determine what fraction of bubble collisions lead to coalescence events, it is necessary to define a collision efficiency. This efficiency will be a function of the contact time between bubbles and the time required for bubbles to coalesce. An expression for the efficiency (λ) is given by Coulaloglou and Tavlarides (1977):

$$\lambda_{ij} = \exp\left(-t_{ij}/\tau_{ij}\right) \tag{16}$$

Here t_{ij} is the time required for coalescence of bubbles of radius r_{bi} and r_{bj}, while τ_{ij} is the contact time for the two bubbles. Coalescence times have been successfully modeled in stagnant fluids by examining the time required for the liquid film between bubbles to thin from an initial thickness to a critical value where rupture occurs. An estimate of the initial thickness of the film in air-water systems is given by Kirkpatrick and Locket (1974) to be 1×10^{-4} m. The final film thickness is typically taken as 1×10^{-8} m (Kim and Lee, 1987). An expression for the thinning of the liquid film between bubbles of equal size is taken from Oolman and Blanch (1986b):

$$\frac{-dh}{dt} = \left\{\frac{8}{R_d^2\rho_l}\left[\frac{-4c}{R_g T}\left(\frac{d\sigma}{dc}\right)^2 + h^2\left(\frac{2\sigma}{r_b} + \frac{A}{6\pi h^3}\right)\right]\right\}^{1/2} \tag{17}$$

where h is the film thickness, R_d is the radius of the liquid disk between the coalescing bubbles, R_g is the gas constant, T is the temperature, A is the Hamaker constant, and c is the concentration of a surfactant species. For the case of distilled water, c is zero and the gas liquid interface is assumed to be mobile (this assumption may not be quite accurate, since even distilled water contains some impurities). The equation is derived from consideration of the flow rate of fluid from the liquid film by capillary pressure, augmented by the Hamaker contribution. The effect of the Hamaker force only becomes appreciable at very low film thicknesses, just prior to rupture. It reflects the mutual attraction of water molecules on opposite sides of the liquid film. Inclusion of this term necessitates a numerical solution for the coalescence time and make the current model cumbersome. Numerical solutions to Eq. 17 showed that for the present study incorporation of this term had only a slight influence on the overall coalescence time. It is therefore neglected in the subsequent analysis. The result of neglecting the Hamaker contribution may be a slight overestimation of the coalescence time. This is partially offset by the fact that coalescence times are increased where there is an appreciable approach velocity (Kirkpatrick and Lockett, 1974), as would be the case in turbulent systems. The effect of bubble deformation by turbulent eddies on the coalescence rate of bubbles is also neglected here. Prediction of the extent of bubble deformation and the subsequent increase in coalescence time due to turbulent eddies is not well understood. In the current analysis, the radius of the liquid disk between coalescing bubbles (R_d) is assumed to be a constant fraction of the bubble radius. Using the above assumptions, the coalescence time can be found by integration of Eq. 17:

$$t_{ij} = \left\{\frac{r_{ij}^3\rho_l}{16\sigma}\right\}^{1/2} \ln\frac{h_o}{h_f} \tag{18}$$

Here h_o is the initial film thickness with h_f is the critical film thickness where rupture occurs. In Eq. 18, R_d has been assumed to be the bubble radius. This approximation is not strictly accurate, however, it is used for simplicity and because more detailed data are not available. It will be shown in the discussion of the coalescence efficiency that inaccuracies here will be compensated in the final expression for the coalescence rate. For the case of bubbles of unequal size, r_b in Eq. 17 has been replaced by the equivalent radius (r_{ij}). The equivalent radius is given by Chesters and Hoffman (1982) as:

$$r_{ij} = \frac{1}{2}\left(\frac{1}{r_{bi}} + \frac{1}{r_{bj}}\right)^{-1} \tag{19}$$

The time that bubbles remain in contact is dependent on the bubble size and the turbulent intensity. High levels of turbulence increase the probability that an eddy will separate particles, while large particle size provides larger contact areas. Levich (1962) provides an estimate of the contact time in turbulent flows:

$$\tau_{ij} = \frac{r_b^{2/3}}{\epsilon^{1/3}} \tag{20}$$

Levich derives Eq. 20 solely from dimensional considerations. The choice of characteristic length is therefore arbitrary and may be considered to be an adjustable variable. Equation 20 may strictly be regarded only as an order of magnitude approximation. Given the sensitivity of the model to this variable, it would be beneficial to have accurate data on particle contact times in turbulent flows. Unfortunately, such data are not available.

Values for the coalescence and contact time may be substituted into Eq. 16 to determine the efficiency. It can now be seen that substitution of the bubble radius for R_d in Eq. 18 does not appreciably alter the results of the model. Incorporation of an alternate expression for R_d would simply result in a small adjustment of the characteristic length employed in Eq. 20. It should therefore be noted that the expression for the coalescence rate will have an implicit adjustable parameter. The development ensures, however, that this parameter will be of the appropriate order of magnitude.

The coalescence rate of bubbles of radii r_{bi} and r_{bj} (Γ_{ij}) is given by the total collision frequency multiplied by the efficiency.

$$\Gamma_{ij} = \left\{\theta_{ij}^T + \theta_{ij}^B + \theta_{ij}^{LS}\right\} \times \exp\left\{-t_{ij}/\tau_{ij}\right\} \tag{21}$$

The overall coalescence rate is then given by:

$$\Gamma_T = \frac{1}{2}\sum_i \sum_j \{(\theta_{ij}^T + \theta_{ij}^B + \theta_{ij}^{LS}) \times \exp(-t_{ij}/\tau_{ij})\} \quad (22)$$

The factor $1/2$ is included to avoid counting coalescence events between bubble pairs twice.

Bubble coalescence rates in turbulent systems containing electrolytes

Salts are found to inhibit bubble coalescence by retarding the thinning of the intervening liquid film between bubble pairs. This phenomenon was examined by Marrucci (1969). At sufficiently high concentrations of salt, the gas-liquid interface between coalescing bubbles is immobilized by the surface tension gradient which results from the thinning process. When this occurs, there is a dramatic increase in the time required for coalescence. The critical concentration of electrolyte required to immobilize the gas-liquid interface of coalescing bubbles is given by Prince and Blanch (1990):

$$c_t = 1.18\left(\frac{B\sigma}{r_b}\right)^{1/2} R_g T\left(\frac{\partial\sigma}{\partial c}\right)^{-2} \quad (23)$$

Film thinning times for bubbles with immobile interfaces are on the order of seconds. The incorporation of transport rates to alleviate the surface tensions gradients and give partial mobility to the gas-liquid interface still result in coalescence times of the order of hundreds of milliseconds (Nicodemo et al., 1969). Since contact times in turbulent dispersions calculated by Eq. 20 are approximately 10 ms, bubble coalescence is not envisaged for systems where the salt concentration is sufficient to immobilize the gas-liquid interface. The coalescence efficiency of bubbles with immobile interfaces is therefore taken to be zero. For salt concentrations lower than the transition value, thinning times may be calculated by solution of Eq. 17. Equation 17 has been numerically integrated for various bubble sizes with the initial and final film thicknesses previously described ($h_o = 10^{-3}$ cm, $h_f = 10^{-6}$ cm). The numerical solutions provide coalescence times for bubbles in electrolyte solutions. These coalescence times may be used in Eq. 22 to calculate coalescence rates.

Bubble break-up

Much of the literature on bubble break-up has focused on the prediction of the maximum stable bubble size, either in stagnant liquids or in isotropic turbulence. There has been little reported on bubble break-up rates under turbulent conditions. Coulaloglou and Tavlarides (1977) developed a model for break-up rates of liquid drops based on the fraction of drops undergoing break-up and the time required for break-up to occur.

$$\beta_i = \left(\frac{1}{\text{breakage time}}\right)\left(\frac{\text{fraction of}}{\text{drops breaking}}\right)$$

$$= K_1 V_{bi}^{-2/9}\,\epsilon^{1/3} \exp\left\{\frac{-K_2\sigma}{\rho_d \epsilon^{2/3} V_{bi}^{5/9}}\right\} \quad (24)$$

Here β_i is the breakage rate of bubbles of volume V_{bi}, ρ_d is the dispersed phase density and K_1 and K_2 are adjustable parameters.

In this derivation, the break-up rate was taken to be a function of the dispersed phase density. However, in gas-liquid systems break-up is governed by the density of the surrounding fluid (Bhavaraju et al., 1978). The lack of an independent measurement of the break-up rate, as well as the use of several adjustable parameters, prevent a direct test of Coulaloglou and Tavlarides' model. Comparison of Eq. 24 with the data obtained in this study for gas-liquid systems, however, yielded values of the break-up rate which were several orders of magnitude lower than experimental observations. Therefore, a model for bubble break-up in turbulent systems is developed below based on the continuous phase density. In this development, the rate of bubble break-up is determined by examining the interaction of bubbles with turbulent eddies.

Collision of bubbles with turbulent eddies

Much of the published literature on bubble break-up is derived from Hinze (1955). Bubble break-up occurs through bubble interactions with turbulent eddies. The eddies responsible for break-up are equal to or marginally smaller than the bubble size. Larger eddies simply transport the bubble without causing break-up, while very small eddies do not contain sufficient energy to affect breakage.

To obtain an expression for the break-up rate of bubbles, we consider the turbulent collision rate of bubbles with eddies of the appropriate size. Again, following Kennard (1938), the collision rate is given by:

$$\theta_{ie} = n_i n_e S_{ie} (\bar{u}_{ti}^2 + \bar{u}_{te}^2)^{1/2} \quad (25)$$

which is analogous to Eq. 1 with the eddy diameter, concentrations and velocity replacing that of one of the bubbles.

To employ this equation, the number of eddies of a particular size must be determined. We assume that the turbulence is isotropic and that the eddy size of interest lies in the inertial subrange. An expression for the number of eddies as a function of wave number for these conditions has been developed by Azbel and Athanasios (1983):

$$\frac{dN(k)}{dk} = \frac{0.1\,k^2}{\rho_l} \quad (26)$$

Here $N(k)$ is the number of eddies of wave number k per mass of fluid. Multiplication by the liquid density yields for the eddy concentration.

In our subsequent analysis we shall be interested in the number of eddies in a discrete size range. The number of eddies within a size category is found by integration of Eq. 26 over the limits of interest. It must be noted that Eq. 26 is only valid for the inertial subrange. The number of eddies predicted by the equation becomes infinitely large as the eddy size approaches zero. Therefore, the expression may not be integrated over the very small eddies which lie in the viscous dissipation range. In practice, therefore, it is necessary to consider an arbitrary size, below which an eddy will not cause breakage. For the present study, this value is set at eddies smaller than 20% of the bubble size. Such eddies are unlikely to contribute significantly to the overall break-up rate. Eddies of a length scale 20% of the bubble diameter possess only 0.5% of the kinetic energy associated with an eddy equivalent to the bubble in size.

Break-up efficiency

Only a certain number of bubble-eddy collisions are likely to result in bubble break-up. The criterion for break-up relates the energy of the eddy to the surface tension forces of the bubble. The balance of disruptive and cohesive forces is generally expressed in terms of the dimensionless Weber number.

$$W_e = \frac{u^2 d_b \rho_l}{\sigma} \tag{27}$$

A critical Weber number will exist at the point where cohesive and disruptive forces balance, resulting in a maximum stable bubble size. Bhavaraju et al. (1978) provide an expression for the maximum stable bubble size in turbulent gas-liquid flows:

$$d_m = 1.12 \frac{\sigma^{0.6}}{(\Psi/V_l)^{0.4} \rho^{0.2}} \left(\frac{\mu_c}{\mu_d}\right)^{0.1} \tag{28}$$

Here d_m is the maximum stable bubble size, V_l is the total volume of liquid and μ_c and μ_d are the viscosities of the continuous and dispersed phases, respectively. From this expression and Eqs. 27 and 7, one may obtain a critical Weber number of 2.3 for air bubbles in water. This is translated into a critical eddy velocity (u_{ci}) for break-up of a bubble of radius r_{bi}:

$$u_{ci} = 1.52(\sigma/r_{bi})^{1/2} \tag{29}$$

It is necessary to determine which eddies have velocities that exceed this value. To do so, an energy distribution function is required. Angelidou et al. (1979) provide such an expression for a random distribution of energy:

$$\chi(E_e) = \frac{1}{\overline{E_e}} \exp\left(\frac{-E_e}{\overline{E_e}}\right) \tag{30}$$

Here $X(E)$ is the energy distribution function and E_e is the kinetic energy of the eddy.

Taking the energy of the eddy as proportional to the square of its velocity yields a function of the following form for the fraction of eddies with sufficient energy to cause rupture (Coulaloglou and Tavlarides, 1977):

$$F(u) = \exp\{-(u_{ci}^2/u_{te}^2)\} \tag{31}$$

where $F(u)$ is the fraction of eddies with sufficient energy to cause rupture and u_{te} is the turbulent velocity of an eddy of radius r_e. This expression is analogous to the collision efficiency for break-up. The break-up rate for a bubble of radius r_{bi} is then given by:

$$\beta_i = \sum_e \{\theta_{ie} \exp[-(u_{ci}^2/u_{te}^2)]\} \tag{32}$$

Here the summation incorporates the contribution to breakup from eddies of various sizes. The total break-up rate for all bubbles is therefore:

$$\beta_T = \sum_i \sum_e \theta_{ie} \exp(-u_{ci}^2/u_{te}^2) \tag{33}$$

Bubble break-up in electrolyte solutions

Bubble break-up in inorganic electrolyte solutions is examined in a manner analogous to that for distilled water or "clean" systems. Break-up is caused by the collision of bubbles with turbulent eddies of the appropriate size and of sufficient energy to cause rupture. Only those eddies equal to and slightly smaller than the bubble size are considered to cause break-up. The critical eddy velocity required to affect bubble break-up is determined from studies of maximum stable bubble size in turbulent flows and isotropic turbulence theory. Walters and Blanch (1986) found that inorganic electrolytes had no significant effect on bubble break-up. Therefore the expression for the break-up rate of bubbles in turbulent solutions of inorganic electrolytes may be taken to be the same as in distilled water.

The negligible effect of electrolytes on bubble break-up rates is due to their very small effect on surface tension. Therefore, the decrease in bubble size reported in salt solutions is believed to be due entirely to their effect on bubble coalescence. It has been shown (Marrucci, 1969) that very small changes in surface characteristics may have a profound effect on the thinning behavior of liquid films due to the gradients which develop in the film during the thinning process.

Despite the previous argument, the addition of electrolytes to gas-liquid contactors will indirectly alter the degree of bubble break-up in these systems. This is due to the effect of salts on bubble size and the concentration of bubbles within the system. Both of these parameters are important in determining the break-up rate of bubbles in turbulent dispersions, as seen by Eqs. 25 and 33.

Model summary and implementation

The preceding sections describe the elements of a predictive model for the coalescence rate of bubbles in turbulent flow based on the collision rate of bubbles and the probability that a collision will result in coalescence. The collision mechanisms resulting from turbulence, buoyancy and laminar shear are considered. The collision efficiency for coalescence is derived through consideration of bubble-bubble contact times and the time required for coalescence. In addition, the expression for bubble break-up rates is developed through consideration of interactions between bubbles and turbulent eddies. Bubbles undergo break-up upon collision with eddies of equal or near equal size possessing sufficient energy to cause rupture. The method of calculating coalescence and break-up rates is summarized below. Model implementation requires that information on the gas flow rate and specific geometry of the system be specified.

Coalescence rates are obtained from the model using Eq. 22. Use of this equation requires calculation of the collision rate of bubbles via the mechanisms discussed, namely turbulence, buoyancy and laminar shear. The turbulent collision rate is calculated from Eq. 8 with use of the energy dissipation rate taken from Eq. 6. Collisions due to buoyancy are obtained from Eq. 9 utilizing the rise velocities of bubbles as described in Eq. 10. The final collision mechanism of laminar shear is calculated from Eq. 11 using the averge shear rate obtained from Eq. 13. The coalescence and contact times of bubbles which occur in Eq. 22 are calculated from Eq. 18 and 20, respectively.

It may be of interest to note that for the experimental conditions used in the current study, the turbulent collision

mechanism dominates. It should also be clear that the relative contribution of buoyancy will diminish as the gas flow rate increases, since both laminar shear and turbulent collisions are functions of the sparge rate. As noted previously, collisions due to laminar shear are absent when the column operates in the homogeneous regime, but become important at higher gas sparge rates when heterogeneous operation is achieved.

The method of obtaining break-up rates may be summarized as follows. The break-up rate is given by Eq. 33, which requires information on the collision rate of bubbles with turbulent eddies. The collision rate is given by Eq. 25. This rate, in turn, is dependent on the velocities of bubbles and eddies, both of which are calculated from Eq. 7. The number of eddies of a particular size is obtained by integrating Eq. 26 over the eddy size range of interest. Also in Eq. 3 are expressions for the eddy turbulent velocity, which is given by Eq. 7, and the critical velocity of an eddy necessary to cause break-up. This latter quantity is obtained from Eq. 29.

In order to utilize the model, it is also necessary to obtain data on bubble size distributions and bubble concentrations. Bubble concentrations can be obtained from gas hold up and bubble size data. Taking the number of bubbles as equal to the volume of gas divided by the average bubble size one obtains:

$$n_i = \frac{\phi R_T^2 H_T}{\frac{4}{3}\bar{r}_{bi}^3} x_i \tag{34}$$

where x_i is the fraction of bubbles with radius r_{bi}.

Representative values of predicted coalescence and break-up rates as a function of bubble volume are shown in Figure 1, with parameters typical of those employed in the present work. The results shown in the figure are calculated using the physical dimensions of the column employed in this study and a superficial gas velocity of 3.5 cm/s. Events are calculated at discrete bubble volumes and a smoothed curve drawn. Both coalescence and break-up are functions of bubble size. Large bubbles are subject to higher breakage rates due to increased eddy collisions and higher collision efficiencies. Coalescence exhibits a weaker size dependence. Larger bubbles have higher collision rates resulting from their increased velocity and collision cross sectional area, however, they have large coalescence times which give rise to smaller coalescence efficiencies.

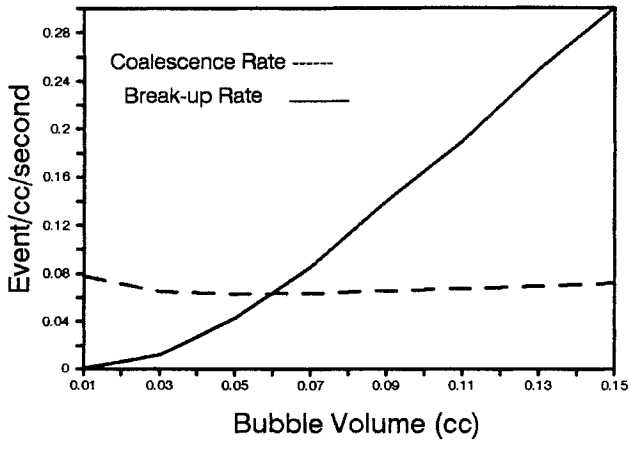

Figure 1. Coalescence and break-up rates as a function of bubble size.

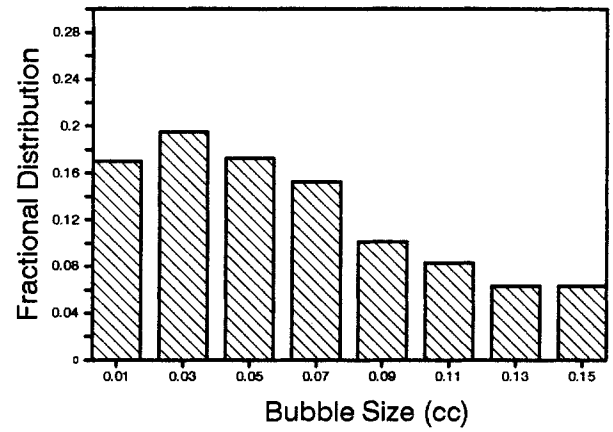

Figure 2. Projected bubble size distribution.

Predictions for bubble size distributions are shown in Figure 2. Calculations are based on Eqs. 22 and 33 using the same parameters as Figure 1. Note that the model, like that of Coulaloglou and Tavlarides (1977), predicts a non-Gaussian distribution of bubble volumes. The current study makes use of a Monte Carlo simulation to determine bubble sizes (see Appendix). In the Monte Carlo program a sample of bubbles with a random size distribution is used to initialize the simulation. This population of bubbles is divided into discrete size categories. Bubbles within a given size category are then chosen at random and subjected to the coalescence and break-up rates predicted by the outlined model for bubbles of that size. The resulting size distribution is recorded after a number of coalescence and break-up events. The procedure is continued until an equilibrium average bubble size is achieved; that is until further iterations produce no change in the average bubble size or bubble size distributions. These model predictions are then compared with experimental data.

Experimental Determination of Bubble Coalescence and Break-up Rates

Experimental apparatus

Direct measurement of coalescence rates in a bubble column was accomplished by recording the mixing of gases within bubbles which occurs whenever two bubbles coalesce. Figure 3

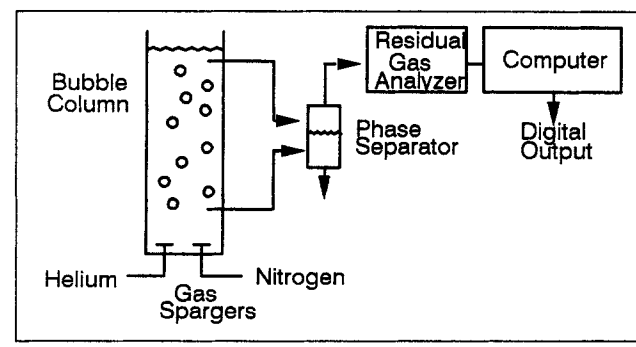

Figure 3. Experimental apparatus.

shows a schematic of the equipment designed to take advantage of this phenomenon. Two insoluble gases, helium and argon, are diluted with nitrogen and fed to separate gas spargers at the base of the bubble column. At this point, the fraction of a particular tracer gas in a bubble relative to the total tracer gas content is either 0 or 1. Therefore a sample of bubbles will give a standard deviation of tracer gas fraction of 0.5. Bubbles coalesce as they ascend the column resulting in the mixing of gases in individual bubbles. This results in a lowering of the standard deviation. The change in the standard deviation between two points may then be related to the number of coalescence events. Samples of bubbles were taken at two distinct points in the column, at 80 and 180 cm above the gas spargers. Gas compositions of individual bubbles at these locations are then determined and used to deduce coalescence behavior between these two points. It is therefore possible to measure coalescence behavior above the region in the column where sparger design dominates the flow pattern and coalescence behavior.

The bubble column consisted of a 27 cm diameter Plexiglass cylinder with a liquid depth of 2 m. The spargers used were two curved stainless steel tubes 20 cm in length, each having six orifices of 2 mm diameter along the upper edge. The two spargers were oriented to maximize radial mixing of the gas streams within the lower section of the bubble column.

The experimental protocol involved filling the column with distilled water or the appropriate electrolyte solution to a height of 2 m. Nitrogen, containing the tracer gases, was fed to the column at a predetermined rate. The system was allowed to come to equilibrium over a period of approximately 5 min. A glass tube of 1-mm inner diameter with a funnel approximately five millimeters wide and five millimeters long was employed to withdraw sample bubbles. Coalescence was minimized during the sampling process by ensuring very short residence times in the funnel. It was found that the hydrostatic pressure of the column provided a sufficient and steady flow of liquid through the sample tube. The rate of flow was adjusted to allow visual observation of the individual bubbles flowing through the glass tubing. The smaller diameter tubing prevented bubbles from overtaking each other in the sample line. Visual observations confirmed that coalescence did not occur during sampling.

The bubbles were drawn from the column into a glass holding coil prior to being fed individually to a residual gas analyzer. Storage time in the coil while the sample was being processed was typically 20 min. Calculations showed that the degree of gas diffusion between bubbles or loss of helium through the glass tubing was negligible during this time period.

The bubbles were then fed individually to a phase separator. The separator was a 10 mm inner diameter vertical chamber containing a hydrophobic Celanese polypropylene membrane. The membrane permitted bubbles to be separated from the liquid phase and fed to the mass spectrometer. The mass spectrometer operated at a pressure of 10^{-5} torr. Since an entire bubble would raise the pressure in the analyzer past tolerable levels, part of the gas sample was discharged through a second vacuum line.

The mass spectrometer was interfaced with a minicomputer which integrated the peak heights of the tracer gases over time, allowing the tracer gas fractions in each bubble to be determined. It was necessary to normalize the peak heights in order to account for the different sensitivity of the gas analyzer to both helium and argon. Samples consisted of approximately 100 bubbles. Experiments were performed using bubbles of known concentration, showing that the described procedure provided accurate measurements of the tracer gas fraction in the bubble samples.

The standard deviation of the tracer gas content was determined for samples from both sampling ports in the column, allowing the determination of coalescence rates between these two points. Samples were also taken from various radial positions in the column and these values were used to obtain a representative bubble sample for that column height. In almost all cases there was good radial mixing and the results were fairly constant across the column. This procedure provided data for the standard deviation in gas composition of bubble samples at two axial points in the column, which was then converted to coalescence events through use of a Monte Carlo simulation. The simulation is a modification of a similar approach used by Oolman and Blanch (1986a). Further details are given in the appendix.

Determination of break-up rates

Determination of bubble break-up rates required data on bubble size and bubble size distributions. It was not found possible to withdraw a sample of bubbles from the column without some bubble break-up occurring in the sampling funnel (while at the same time ensuring no coalescence in the sampling funnel). Consequently, bubble size data were taken photographically at the gas rates employed for the coalescence measurements without relying on the actual bubble samples withdrawn from the column. Viewing windows were constructed on the bubble column that consisted of a reservoir of water with a flat window facing outward. Using these windows, photographs of bubble size could be taken without visual distortion caused by the curvature of the bubble column. A scale was inserted into the column to calculate actual bubble dimensions in the photographs. The photographs were then enlarged and bubble sizes manually measured. It was assumed that the bubble were oblate spheroids, and the major and minor axes were used to compute bubble volumes.

Bubble size results in conjunction with coalescence data were used to determine bubble break-up rates through use of a simple population balance. A number balance of bubbles is written noting that coalescence results in the loss of one bubble per coalescence event and that one bubble is produced per break-up event:

$$\beta_T = \frac{N_{bf} - N_{bi}}{\pi R_T^2 L_p t_r} + \Gamma_T \tag{35}$$

Here N_{bi} and N_{bf} are the initial and final number of bubbles, respectively. Note that Eq. 35 is general and does not require information on the size dependency of the coalescence and break-up processes.

It is more useful for the break-up rate to be expressed in terms of experimentally measured variables, namely the average bubble size rather than the bubble number. Equation 35 may be

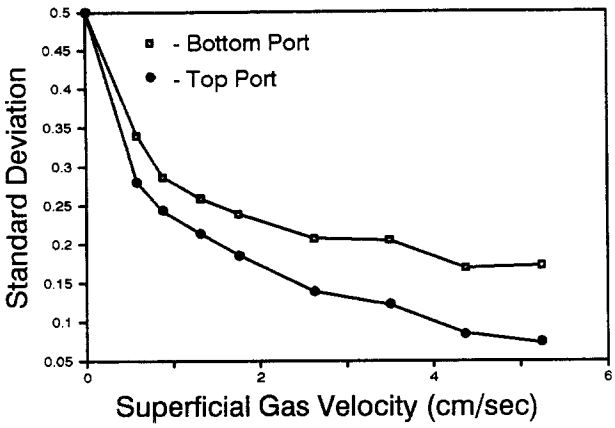

Figure 4. Standard deviation vs. gas sparge rate.

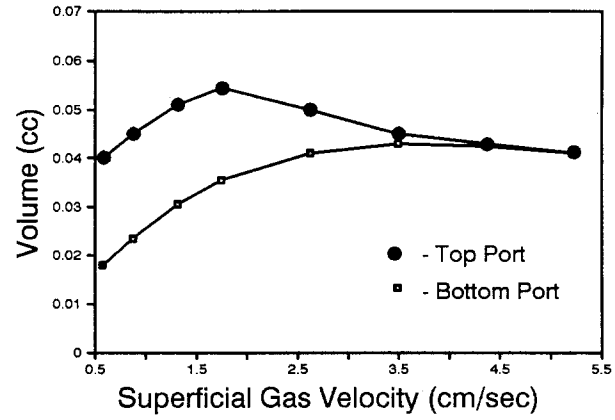

Figure 6. Bubble size vs. gas sparge rate, expressed as bubble volume.

rearranged to give:

$$\beta_T = \Gamma_T + \frac{\phi H_T}{L_p t_r}\left(\frac{1}{\overline{V}_{bf}} - \frac{1}{\overline{V}_{bi}}\right) \tag{36}$$

Here $\overline{V}_{bi}$ and $\overline{V}_{bf}$ are the initial and final average bubble size between ports. It may be seen that Eq. 36 gives equal coalescence and break-up rates for the case where no change in bubble size occurs.

Results and Discussion

Distilled water

The standard deviation of tracer gas concentration in the bubble samples for various gas rates is shown in Figure 4. These are converted to bubble coalescence events per volume per second in Figure 5 using the method outlined in the appendix. Also shown in Figure 5 is the prediction of Eq. 22. The model predicts coalescence behavior quite closely. The increase in coalescence rates at higher gas throughputs is due to the dramatic increase in collision events, both because of increased bubble concentrations and through higher relative velocities. Offsetting this to some degree is the reduced bubble contact time associated with higher turbulent intensities in the liquid.

The bubble concentrations in Eq. 22 were determined from data on bubble size and experimental values for the gas holdup as described in Eq. 34. Average bubble volumes at the two axial positions in the bubble column, corrected for differences in hydrostatic pressure, are given as a function of gas rates in Figure 6. As can be seen, only at superficial velocities of 4.4 and 5.2 cm per second was an equilibrium bubble size achieved.

There is a maximum in the bubble size as a function of gas rate due to the competing effects of coalescence and break-up. At the low gas flow rates, increasing the gas flow leads to higher bubble collision rates and therefore to more coalescence. As the turbulent intensity increases, however, bubble break-up becomes prevalent, leading to a reduction in average size.

Results for the rate of bubble breakup are shown in Figure 7. Break-up is seen to increase dramatically with increased gas rate. This is due to the increase in the number of eddies with sufficient energy to rupture the bubble. Figure 7 also presents a comparison of the experimental data with the predictions of Eq. 33. It is not possible to extend Eq. 33 over the complete range of eddy sizes, since the expression for eddy number is only applicable to eddies in the inertial subrange. Therefore, eddies smaller than 20% of the bubble size were ignored. It is unlikely, however, that such eddies would contribute significantly to the

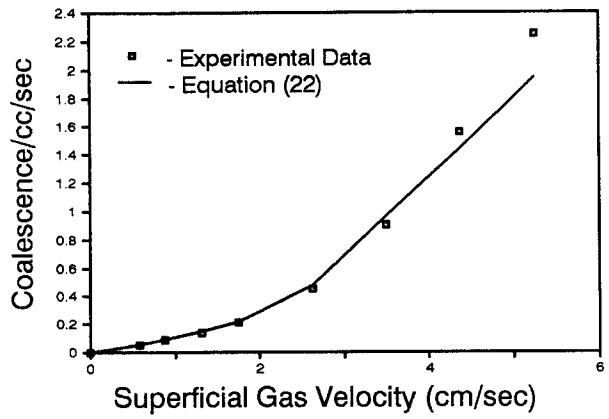

Figure 5. Bubble coalescence vs. gas sparge rate.

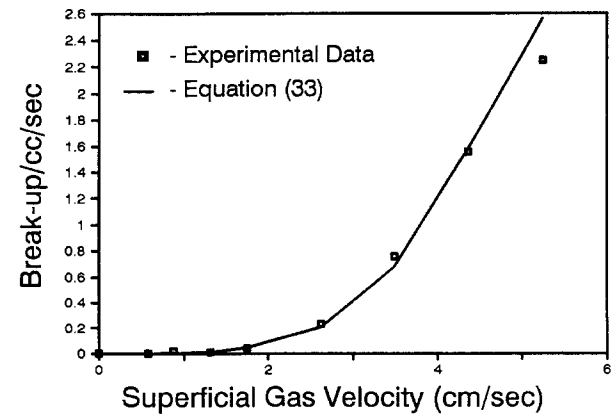

Figure 7. Bubble break-up vs. gas sparge rate.

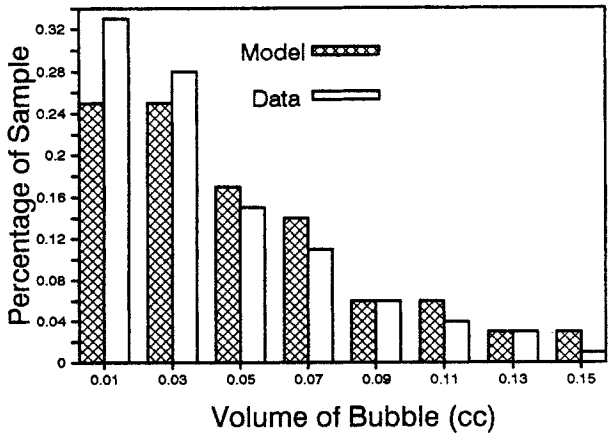

Figure 8. Bubble size distribution.

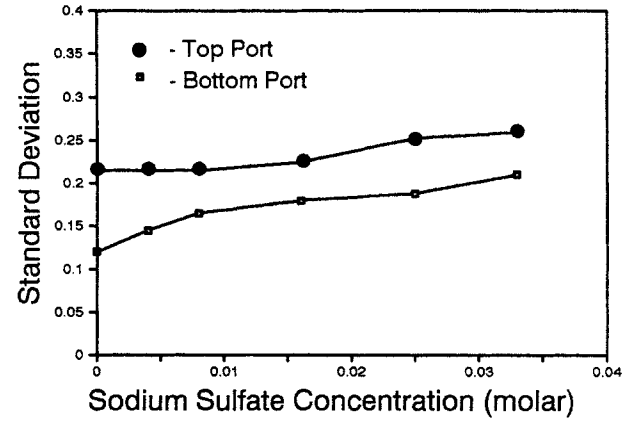

Figure 10. Standard deviation of bubble sample vs. Na_2SO_4 concentration.

overall break-up rate. Given these restrictions, it is seen that Eq. 33 predicts break-up rates quite well.

Both the average bubble size and the bubble size distribution are predicted from the model by repetition of coalescence and break-up events until an equilibrium state is reached. Therefore, the predicted bubble sizes should only be compared to those experimental systems where this equilibrium has been achieved. For the present study, only the highest two gas rates, 4.4 and 5.2 cm per second, show evidence that the bubble size has stabilized. Therefore, only data from those two experiments may be compared to the model. The predicted values for the average bubble radius for these two experiments are 0.24 and 0.23 cm, respectively. The experimental value for both gas rates is 0.22 cm.

The experimental bubble size distribution for a superficial gas velocity of 5.2 cm/s is given in Figure 8 with a comparison from the Monte-Carlo simulation. In this simulation, the break-up process was considered to occur by breakage of a bubble into two daughter bubbles of random size. It is seen that the model agreement with the experimental results is good. It may be noted that the model predicts values less than the experimental values for very small bubbles. This may be due to the fact that break-up may not be the simple binary split that has been assumed. Prince et al. (1989) and others have noted that bubble break-up is often accompanied by the production of two primary drops and a number of smaller fragments. Incorporation of this effect would significantly alter the number of smaller bubbles predicted by the model.

Electrolyte solutions

Coalescence and break-up rates for bubbles in electrolyte solutions were also analyzed. A superficial velocity of 5.2 cm/s was used in these experiments. The standard deviation of the concentration of tracer gas in the bubble samples for NaCl solutions is shown in Figure 9. Similar data for Na_2SO_4 solutions are given in Figure 10. The standard deviation is seen to rise for both ports with the addition of electrolyte, showing a reduction in the degree of bubble coalescence. Data on the actual coalescence rates of bubbles, reported in terms of coalescence event per bubble per second, are shown in Figures 11 and 12 for NaCl and Na_2SO_4 solutions, respectively. The figures show the reduction of coalescence rates with the addition of salts. Examination of Figures 11 and 12 show that sodium sulfate is more effective at reducing coalescence than NaCl at low concentrations. This is partially due to the larger effect of Na_2SO_4 on the surface tension. Even at constant values of $c(\partial^2\sigma/\partial c^2)$, however,

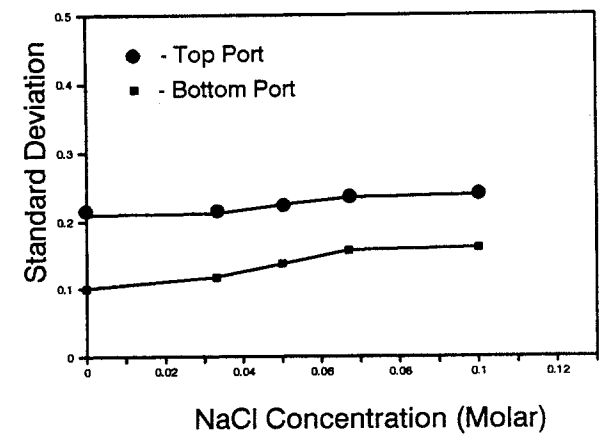

Figure 9. Standard deviation of bubble sample vs. NaCl concentration.

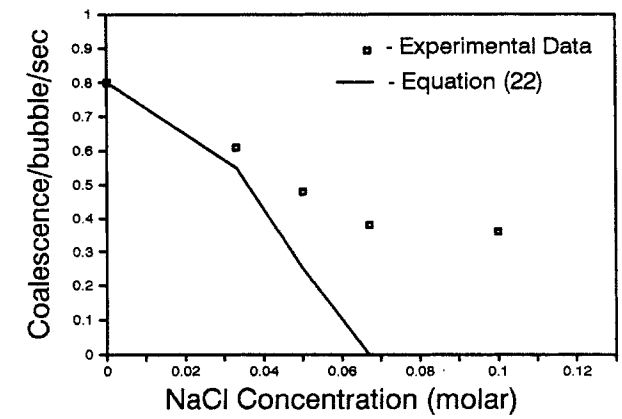

Figure 11. Bubble coalescence rate vs. NaCl concentration.

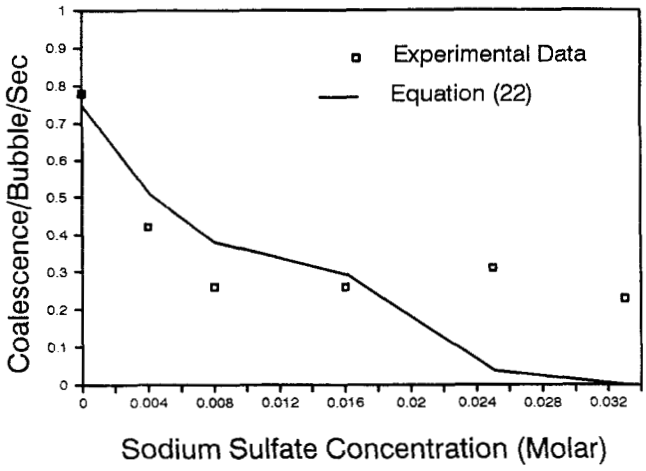

Figure 12. Bubble coalescence rate vs. Na_2SO_4 concentration.

for which the model predicts equal coalescence times, sodium sulfate is seen to be more effective at inhibiting coalescence. This may be due to the lower diffusivity of sodium sulfate (1.14×10^{-5} vs. 1.55×10^{-5} cm^2/s for NaCl) and therefore its lessened ability to relieve surface tension gradients during film thinning. Examination of Eq. 16 shows that small changes in the thinning time may have large effects on the coalescence efficiency of collision and hence the coalescence rate.

Figures 11 and 12 also show the comparison of Eq. 22 with data for bubble coalescence rates in NaCl and Na_2SO_4 solutions. Here the thinning times for coalescence were calculated from numerical solutions of Eq. 17 with the value of B taken as 1.5×10^{-19} erg · cm (Black et al., 1960). It is seen that the model predicts no coalescence for the higher salt concentrations. This is due to the assumption that no coalescence occurs once the salt concentration is high enough to immobilize the gas-liquid interface.

It can be seen that the present model for bubble coalescence rates in turbulent electrolyte solutions is inadequate, particularly for the higher salt concentrations. While the transition concentration of salts in stagnant liquids is well correlated by

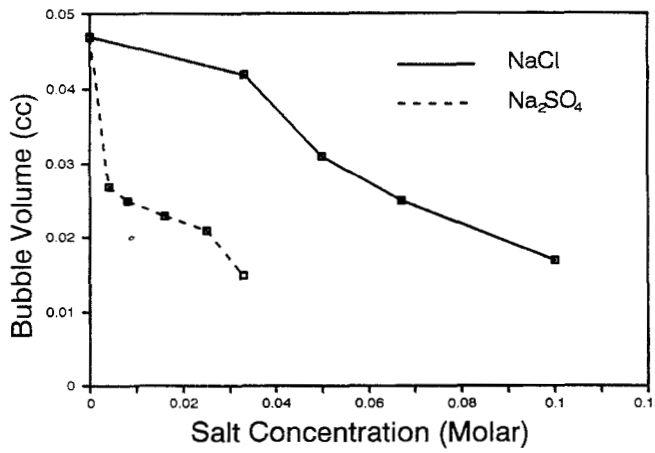

Figure 13. Bubble volume vs. NaCl and Na_2SO_4 concentrations.

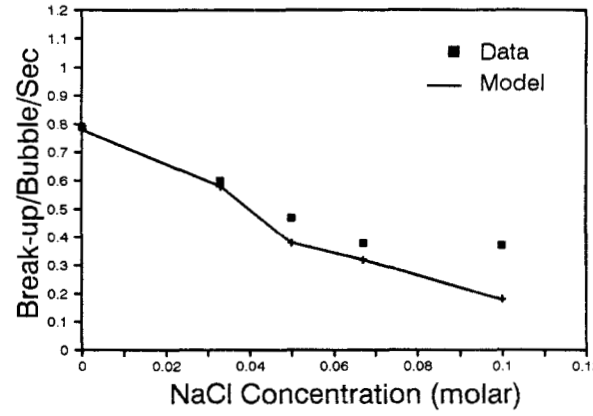

Figure 14. Bubble break-up in sodium chloride solutions.

the current approach, it may not be applicable in turbulent systems where the hydrodynamics affect surface properties and the energy of bubble collisions. Bubble motion leads to uneven distributions of surfactants on rising bubbles, thereby influencing the surface mobility and rise velocity. The possibility also exists that the turbulent motion of bubbles or eddies may alter the surface distribution for salts as well, thus making the value of the surface excess at the point of bubble collision uncertain. In addition, the hydrodynamic environment may alter the amount of salt required to immobilize the bubble interface. These factors pose additional complications in predicting the effect of surface contaminants on bubble coalescence rates in turbulent systems.

The reduction in coalescence rates is reflected in the change in bubble size. Average bubble sizes for various concentrations of NaCl and Na_2SO_4 solutions are shown in Figure 13. It is seen that the fall in bubble volumes follows very closely the reduction in coalescence rates.

Bubble break-up rates per bubble per second for NaCl and Na_2SO_4 solutions are shown in Figures 14 and 15, respectively. Also shown are the model predictions using Eq. 33. It is seen that the model closely matches the data for bubble break-up. This is particularly encouraging in view of the fact that no parameters have been adjusted from the model developed for distilled water to fit the bubble break-up data in the electrolyte

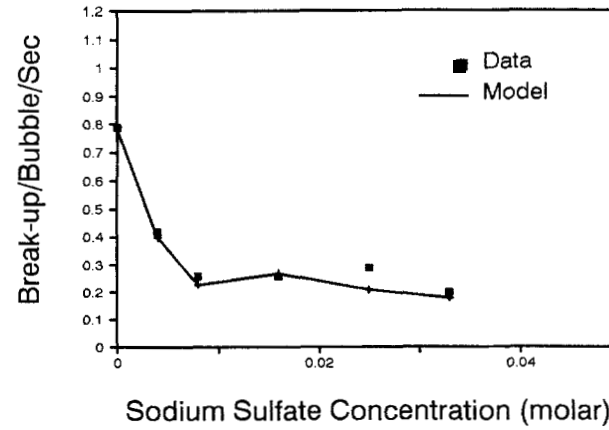

Figure 15. Bubble break-up in sodium sulfate solutions.

solutions. This further supports the hypothesis that bubble break-up rates are not affected by salt concentration, except in so far as electrolytes alter the bubble size.

Conclusions

A model for bubble coalescence and break-up rates has been developed which compares favorably with experimental results in distilled water. The coalescence model considers the collision rate of bubbles and the likelihood of collisions resulting in coalescence. Collisions due to turbulence, buoyancy and laminar shear have been considered. The coalescence efficiency was determined by evaluation of the time required for coalescence and the contact time of two bubbles in turbulent flow. A simplified model for film thinning, neglecting the Hamaker contribution and the approach velocity between bubbles, was employed to determine the coalescence time. Bubble break-up was modeled by examination of bubble interaction with turbulent eddies. Break-up was assumed to occur when bubbles encountered eddies of appropriate size and sufficient energy to cause rupture. In all cases, the turbulence was assumed to be isotropic and the particles were considered to lie in the inertial subrange.

In addition to predicting individual coalescence and break-up rates, the model has been shown to predict equilibrium bubble size and bubble size distributions. The favorable comparison of data with the model suggest that the model may be used to predict bubble size, size distribution and dispersed phase mixing rates in "clean" systems. The model also provides a framework to optimize reactor performance with regard to mass transfer rates.

A primary contribution of the present study is the development of a method to measure bubble coalescence and break-up rates. Coalescence rates were determined from the mixing of tracer gases in individual bubbles that results from coalescence. A Monte-Carlo simulation was developed which allowed for the quantitative assessment of coalescence rates from changes in the standard deviation of the gas composition of bubble samples. Thus a quantitative measure of bubble coalescence in turbulent systems has been obtained. It was shown that bubble break-up rates could be determined from coalescence data in conjunction with information on bubble size thorough use of a simple population balance.

The extension of the model for bubble coalescence and break-up to systems containing inorganic electrolytes is examined. This extension is of significant practical importance due to the prevalence of such systems in industrial processes. It is seen that bubble break-up rates in the electrolyte solutions examined in this work may be predicted using the model developed for clean systems. This is consistent with previous studies of bubble break-up in salt solutions. However, the present work provides experimental verification of this phenomena in turbulent systems, and presents a quantitative description of the reduction in the bubble break-up rate with the addition of electrolytes.

Inorganic electrolytes were found to significantly decrease the degree of bubble coalescence in turbulent gas-liquid dispersions. Such results are consistent with expectations from previous studies, but the reduction in bubble coalescence rates with the addition of salts has been directly measured here. It was found that experimentally measured coalescence rates in electrolyte solutions could not be predicted by the current model for salt levels beyond the predicted transition concentration. This is attributed to the effects of turbulence on surface mobility, the dynamics of bubble collisions and the level of salt at the gas-liquid interface between coalescing bubbles.

While the proposed model adequately predicts bubble dispersion properties in distilled water, the scant amount of independent data for bubble coalescence and break-up rates makes assessment of a model difficult. Various aspects of the model deserve further consideration. There is a lack of information on particle contact times in turbulent flows, necessitating the use of what is in effect an adjustable parameter. The effect of the approach velocity on bubble coalescence times is poorly understood. In addition, the assumptions of plane parallel flow and a constant film radius between coalescing bubbles may well be oversimplifications which deserve additional treatment. In the area of bubble break-up, refinements in the number of daughter bubbles resulting from break-up and their size distribution may need to be included in the present model. Finally, the effects of turbulence on the transition concentration of salt as well as its effect on coalescence rates needs to be determined.

Notation

A = Hamaker constant, erg
B = retarded Van der Waals coefficient, erg · cm
c = concentration of surfactant, mol/L
c_t = transition salt concentration, mol/L
d_b = bubble diameter, m
d_m = maximum stable bubble size, m
D_T = tank diameter, m
E_e = eddy kinetic energy, kg · m^2/s^2
$F(u)$ = eddy velocity distribution function
F_H = force of attraction, dyne
g = gravitational constant
h = film thickness between coalescing bubbles, m
H_T = unaerated liquid height, m
k = wave number, m^{-1}
K_1, K_2 = adjustable parameters (Eq. 24)
k_b = wave number corresponding to bubble size, m^{-1}
k_d = wave number of viscous dissipation, m^{-1}
k_e = wave number of energy containing eddies, m^{-1}
L_p = length between sampling ports in column, m
N = eddy concentration per mass, kg^{-1}
n = eddy or bubble concentration per volume, m^{-3}
N_b = total number of bubbles
P = pressure, atm
Q = volumetric sparge rate measured at the pressure of the base of the bubble column, m^3/s
R = radial coordinate of bubble column, m
R_d = radius of contact area between bubbles
r_b = rubble radius, m
R_g = gas constant
R_T = tank radius, m
S = collision cross sectional area, m^2
Sx = gas fraction standard deviation
t = coalescence time, s
T = temperature
t_r = residence time of bubbles between sampling ports, s
u_c = critical eddy velocity for bubble break-up, m/s
U_g = superficial gas velocity, m/s
U_l = liquid circulation velocity, m/s
$U_{l,\max}$ = center line circulation velocity, m/s
u_r = bubble rise velocity, m/s
u_t = turbulent velocity, m/s
v = velocity, cm/s
V_b = bubble volume, m^3
V_{bc} = volume of bubble undergoing coalescence, m^3
V_{gc} = volume of gas undergoing coalescence, m^3
V_{gT} = total volume of gas, m^3
V_l = total volume of liquid, m^3
We = Weber number defined by Eq. 26

x = volume fraction of tracer gas in bubble
x_i = fraction of particles of radius r_{bi}

Greek letters

α = fractional radial tank position of stagnation point
β = break-up rate, $m^{-3} \cdot s^{-1}$
χ = eddy energy distribution function
ϵ = energy dissipation rate per mass, m^2/s^2
Γ = bubble coalescence rate, $m^{-3} \cdot s^{-1}$
γ = local shear rate, s^{-1}
λ = coalescence efficiency
μ = continuous phase viscosity, g/cm · s
μ_c = continuous phase viscosity, kg/m · s
μ_d = dispersed phase viscosity, kg/m · s
ν = kinematic viscosity, m^2/s
ν_t = kinematic viscosity defined by equation 15, m^2/s
ϕ = gas holdup
ψ = power input, kg · m^2/s^3
ρ = density, kg/m^3
σ = surface tension, kg/s^2
τ = bubble contact time, s
θ^B = buoyancy driven collision rate, $m^{-3} \cdot s^{-1}$
θ^{LS} = collision rate due to laminar shear, $m^{-3} \cdot s^{-1}$
θ^T = collision rate due to turbulence, $m^{-3} \cdot s^{-1}$

Subscripts

b = bubble
c = continuous phase
d = dispersed phase
e = eddy
f = final
g = gas
i,j = particle i,j
l = liquid
T = tank
T = total

Superscripts

* = rate measured per length between ports
– = mean value

Literature Cited

Angelidou, C., M. Psimopoulos, and G. J. Jameson, "Size Distribution Functions of Dispersions," *Chem. Eng. Sci.*, **34,** 671 (1979).
Azbel, D., and I. L. Athanasios, "A Mechanism of Liquid Entrainment," p. 473, *Handbook of Fluids in Motion,* N. Cheremisinoff, ed., Ann Arbor Science Publishers, Ann Arbor, MI (1983).
Batchelor, G. K., *The Theory of Homogeneous Turbulence,* Cambridge University Press, Cambridge (1953).
Black, W., J. G. V. de Jongh, J. T. G. Overbeek, and M. J. Sparnaay, *Trans. Faraday Soc.*, **56,** 1597 (1960).
Bhavaraju, S. M., T. W. F. Russell, and H. W. Blanch, "The Design of Gas Sparged Devices for Viscous Liquid Systems," *AIChE J.*, **24,** 3 (1978).
Calderbank, P. H., M. B. Moo-Young, and R. Bibbly, "Coalescence in Bubble Reactors and Absorbers," *Proc. Euro. Symp. on Chem. Reaction Eng.*, 91 (1964).
Chesters, A. K., and G. Hofman, "Bubble Coalescence in Pure Liquids," *Appl. Scientif. Res.*, **38,** 353 (1982).
Clift, R., J. R. Grace, and M. E. Weber, *Bubbles, Drops and Particles,* Academic Press, New York (1978).
Coulaloglou, C. A., and L. L. Tavlarides, "Description of Interaction Processes in Agitated Liquid-Liquid Dispersions," *Chem. Eng. Sci.*, **32,** 1289 (1977).
Friedlander, S. K., *Smoke, Dust and Haze,* Wiley, New York, (1977).
Hinze, J. O., "Fundamentals of the Hydrodynamic Mechanism of Splitting in Dispersion Processes," *AIChE J.*, **1,** 289 (1955).
Keitel, G. and O. Ulfert, "The Effect of Solutes on Bubble Size in Air-Water Dispersions," *Chem. Eng. Comm.*, **17,** 85 (1982).
Kennard, E. H., *Kinetic Theory of Gases,* McGraw-Hill, New York (1938).
Kim, W. K., and K. L. Lee, "Coalescence Behavior of Two Bubbles in Stagnant Liquids," *J. of Chem. Eng. of Japan,* **20,** 449 (1987).
Kirkpatrick, R. D., and M. J. Lockett, "The Influence of Approach Velocity on Bubble Coalescence," *Chem. Eng. Sci.*, **29,** 2363 (1974).
Levich, V. G., *Physicochemical Hydrodynamics,* Prentice Hall, Englewood Cliffs, NJ (1962).
Marrucci, G., "A Theory of Coalescence," *Chem. Eng. Sci.*, **24,** 975 (1969).
Marrucci, G. and L. Nicodemo, "Coalescence of Gas Bubbles in Aqueous Solutions of Inorganic Electrolytes," *Chem. Eng. Sci.*, **22,** 1257 (1967).
Miyauchi, T., and C. N. Shyu, "Fluid Flow in Gas Bubble Columns," *Kagaku Kogaku,* **34,** 958 (1970).
Nicodemo, L., G. Marrucci, and D. Acierno, "Bubble Pair Coalescence in Electrolyte Solutions," *Ing. Chim. It.*, **8,** 1 (1972).
Oolman, T., and H. W. Blanch, "Bubble Coalescence in Air-Sparged Bioreactors," *Biotech. Bioeng.*, **28,** 578 (1986a).
———, "Bubble Coalescence Stagnant Liquids," *Chem. Eng. Commun.*, **43,** 237 (1986b).
Prince, M., and H. W. Blanch, "Transition Electrolyte Concentrations for Bubble Coalescence," *AIChE J.*, **36,** 1425 (Sept., 1990).
Prince, M., J. Walters, and H. W. Blanch, "Bubble Break-Up in Air Sparged Biochemical Reactors," *First Generation of Bioprocess Engineering,* T. K. Ghose, ed., 160 (1989).
Ross, S. L., F. H. Verhoff, and R. L. Curl, "Droplet Breakage and Coalescence Processes in an Agitated Dispersion. w. Measurement and Interpretation of Mixing Experiments," *Ind. and Eng. Chem. Fund.*, **17,** 101 (1978).
Rotta, J. C., *Turbulente Stromungen,* B. G. Teubner, Stuttgart (1972).
Shah, Y. T., and W. D. Deckwer, "Hydrodynamics of Bubble Columns," *Handbook of Fluids in Motion,* Ann Arbor Science Publishers, Ann Arbor, MI, 583 (1983)
Swift, D. L., and S. K. Friedlander, "The Coagulation of Hydrosols by Brownian Motion," *J. Colloid Sci.*, **19,** 621 (1964).
Ueyama, K., and T. Miyauchi, "Properties of Recirculation Turbulent Two Phase Flow in Gas Bubble Columns," *AIChE J.*, **25,** 258 (Mar., 1979).
Valentas, K. J., and N. R. Amundson, "Breakage and Coalescence in Dispersed Phase Systems," *I and EC Fund.*, **5,** 533 (1966).
Walters, J., and H. W. Blanch, "Liquid Circulation Patterns and their Effect on Gas Holdup and Axial Mixing in Bubble Columns," *Chem. Eng. Commun.*, **19,** 243 (1983).
———, "Bubble Break-Up in Gas-Liquid Bioreactors: Break-Up in Turbulent Flows," *Chem. Eng. J.*, **32,** B7 (1986).

Appendix: Monte Carlo Simulation to Determine Coalescence Rates

Coalescence rates as a function of gas phase mixing were determined through use of a Monte Carlo simulation. This method allowed for quantitative analysis of coalescence events as a function of changes in the tracer gas fraction standard deviation. A schematic of the simulation procedure is shown in Figure 1A.

An initial sample of "bubbles" with assigned tracer gas concentrations was entered into the simulation to give the standard deviation (Sx) of an experimental sample of bubbles taken at the lower port in the column. It was found that the specific fractions or combination of fractions of tracer gas chosen did not alter the final result of the coalescence rate, so long as the chosen fraction distribution produced the same value of the initial standard deviation. Bubble pairs in the array were then randomly chosen to undergo coalescence events. The resulting concentration and size of the new bubble were determined through simple mass balances:

$$C_{b3} = \frac{(C_{b1} V_{b1} + C_{b2} V_{b2})}{V_{b1} + V_{b2}}; \quad V_{b3} = V_{b1} + V_{b2} \qquad \text{(A1)}$$

where C_b is the concentration of tracer gas in the bubble.

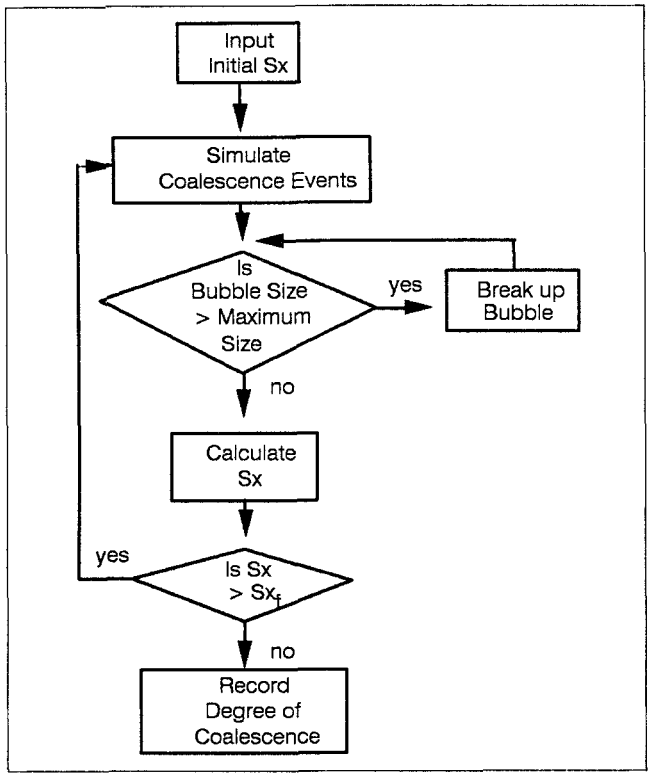

Figure A1. Flowsheet of Monte Carlo simulation.

If the size of the new bubble was greater than arbitrary maximum, the bubble was broken into two randomly sized daughter bubbles. The larger resultant bubble was checked again for excessive size and the break-up procedure was repeated until all daughter bubbles were sufficiently small. The value for the maximum stable bubble size in the simulation could be altered to give various degrees of bubble break-up. This information could then be used to test the effect of the degree of bubble break-up on the simulation results for coalescence rates. The coalescence simulation was continued until the standard deviation of the sample reached that of the population of bubbles taken from the upper port of the bubble column (Sx_f). The total number of coalescence and break-up events were normalized by the number of bubbles in the sample and compared to the changes in the standard deviation of gas composition. The degree of coalescence as a function of gas mixing could then be determined.

Oolman and Blanch (1986a) used a similar technique to provide an explicit empirical relationship between coalescence events and changes in standard deviation. Their formulation is applicable to systems where an equilibrium bubble size has been reached, i.e., where coalescence and break-up rates are identical. These authors assumed that break-up occurred for all bubbles beyond a certain maximum size. The present work extends this model to the general case where the equilibrium bubble size has not been reached and where the mode and degree of break-up need not be specified. A reliance on break-up rates in determining coalescence phenomena is undesirable since the rate and mode of break-up are not known *a prioi*.

While bubble break-up does not affect the gas composition of individual bubbles, it does change the standard deviation of the tracer gas content of the sample by altering the sample size and the distribution of tracer gas fractions in the sample. In addition, by changing bubble size, break-up influences the resulting composition of coalesced bubbles, as may be seen from Eq. A1. The existence of this break-up dependence on coalescence events in the simulation is shown in Table A1. The degree of break-up was altered by assuming different values for the maximum stable bubble size in the simulation. It is seen that the coalescence events per bubble vary significantly for the different assumed degrees of break-up. Therefore, in order to use this approach, the exact degree of break-up would need to be known. To circumvent this dependence, a modified expression for the standard deviation was used, in which tracer gas fractions were weighted by the bubble size:

$$Sx = \left\{ \frac{\sum (V_b)(x)^2}{\sum V_b} - \left[\frac{\sum (V_b)(x)}{\sum V_b} \right]^2 \right\}^{0.5} \qquad \text{(A2)}$$

where x is the volume fraction of argon or helium in the bubble.

In order to eliminate the break-up dependence, it was also necessary to report coalescence data in terms of the volume fraction of gas rather than the number of bubbles coalesced. The insensitivity of this variable to the degree of break-up is demonstrated in Table A1. Volume fractions greater than one indicate that on average bubbles undergo multiple coalescence events. The volume fraction of gas coalesced is easily monitored in the simulation program. This variable is inconvenient for hydrodynamic modeling, however, where coalescence and break-up rates per bubble are required. Equation A3 may be used to convert coalescence rates to a per bubble basis, assuming that the number of bubbles is equal to the volume of gas divided by the average bubble size:

$$\Gamma_T^* = \bar{n}_b \frac{V_{gc}}{V_{gT}} \frac{\overline{V}_b}{\overline{V}_{bc}} \qquad \text{(A3)}$$

where Γ_T^* is the coalescence rate per bubble between sampling ports and $\bar{n}_b$ is the average bubble concentration. V_{gc} is the volume of gas coalesced, V_{gT} is the total volume of gas in the system, $\overline{V}_b$ is the average bubble size and $\overline{V}_{bc}$ is the average volume of the bubbles undergoing coalescence.

Since coalescence is size-dependent, the ratio of the average bubble size relative to the average size of a bubble undergoing coalescence in Eq. A3 need not be unity. In order to determine this value, it was necessary to calculate the average size of bubbles coalescing in comparison to the average bubble size in a sample. This was accomplished by calculating the coalescence rate for bubbles of various sizes using Eq. 21. The value for the

Table A1. Monte Carlo Simulation Results

Gas Rate L/s	Break-Up Rate per Bubble	Coalescence Rate per Bubble	Volume Fraction Coalesced
0.25	0.72	0.46	1.05
0.25	0.30	0.61	1.06
0.25	0.09	0.72	1.08

final ratio in Eq. A3 was then calculated from:

$$\frac{\overline{V}_b}{\overline{V}_{bc}} = \frac{\overline{V}_b \sum_i \sum_j \Gamma_{ij}}{\sum_i \sum_j \Gamma_{ij} V_{bi}} \tag{A4}$$

Use of Eq. A4 in conjunction with the Monte-Carlo simulation allowed the determination of coalescence rates per bubble by a method which was independent of the rate of bubble break-up. It was not possible to correlate coalescence behavior using a simple empirical expression of the type given by Oolman and Blanch (1986a). Instead, changes in the standard deviation of tracer gas concentrations for individual experimental runs were converted to coalescence rates using the described procedure.

Experimental coalescence rates were measured as a function of the distance between the sample ports in the bubble column. It is more useful to convert these values to a unit time basis. The average resident time of a bubble between ports was calculated from:

$$t_r = L_p \frac{\phi}{U_g} \tag{A5}$$

where L_p is the distance between ports, and U_g is the superficial gas velocity. The coalescence rate per length between sampling ports may be converted to coalescence per unit time from:

$$\Gamma_T = \Gamma_T^* \frac{L_p}{t_r} \tag{A6}$$

The value of Γ_T is the experimentally determined overall coalescence rate.

Manuscript received June 27, 1989, and revision received July 25, 1990.